Optics Letters

Polarization diversity phase modulator for measuring frequency-bin entanglement of a biphoton frequency comb in a depolarized channel

Oscar E. Sandoval,[1,†] Navin B. Lingaraju,[1,†,*] Poolad Imany,[1] Daniel E. Leaird,[1] Michael Brodsky,[2] and Andrew M. Weiner[1]

[1]School of Electrical and Computer Engineering, Purdue University and Purdue Quantum Science and Engineering Institute, 465 Northwestern Avenue, West Lafayette, Indiana 47907, USA
[2]U.S. Army Research Laboratory, Adelphi, Maryland 20783, USA
*Corresponding author: nlingara@purdue.edu

Received 16 January 2019; revised 27 February 2019; accepted 27 February 2019; posted 28 February 2019 (Doc. ID 357908); published 22 March 2019

Phase modulation has emerged as a technique to create and manipulate high-dimensional frequency-bin entanglement. A necessary step to extending this technique to depolarized channels, such as those in a quantum networking environment, is the ability to perform phase modulation independent of photon polarization. This is also necessary to harness hyperentanglement in the polarization and frequency degrees of freedom for operations such as Bell state discrimination. However, practical phase modulators are generally sensitive to the polarization of light, and this makes them unsuited to such applications. We overcome this limitation by implementing a polarization diversity scheme to measure frequency-bin entanglement for arbitrary orientations of co- and cross-polarized time-energy entangled photon pairs.

https://doi.org/10.1364/OL.44.001674

Polarization-entangled photons are a popular choice for quantum networking protocols owing to their compatibility with standard telecommunications equipment. Full Bell state discrimination is a prerequisite for superdense coding [1] and teleportation [2]. However, entanglement in one degree of freedom alone is insufficient to perform a full Bell state analysis with a single joint measurement using linear optics. Entanglement in a second degree of freedom has been used to resolve this limitation [1–4].

However, entanglement in the frequency degree of freedom, which is compatible with modern fiber-optic networks, has largely been untapped as a resource for quantum communication. Recently, there has been work outlining ways to perform quantum information processing in the spectral domain using only phase modulators (PMs) and Fourier transform pulse shapers [5]. Furthermore, on-chip microresonators have been shown to be an excellent source for generating time-energy entangled photon pairs [6,7]. One state that is of particular interest is the biphoton frequency comb (BFC)—a coherent superposition state of N-energy matched comb line pairs. If α_k represents the complex amplitude of the kth comb line pair, the general state of a BFC can be written as [8]

$$|\Psi\rangle_{\mathrm{BFC}} = \sum_{k=1}^{N} \alpha_k |k, k\rangle_{SI}. \tag{1}$$

Recent work has shown that electro-optic phase modulation can be used to mix frequencies from different modes and carry out two-photon interferometry that is sensitive to the phase on comb line pairs [6–8], thereby establishing high-dimensional frequency-bin entanglement. However, PMs—whether based on the linear electro-optic effect in $\chi^{(2)}$ materials [9,10], the carrier dispersion effect in silicon [11], or resonant cavities [12]—are sensitive to the polarization of light. Therefore, harnessing hyperentanglement in the polarization and frequency degrees of freedom, for use over fiber-optic networks, requires a polarization diversity scheme capable of measuring frequency-bin entanglement regardless of photon polarization.

The scheme used to achieve polarization-independent phase modulation is shown in Fig. 1. The polarization diversity phase modulator (PDPM) comprises two fiber-based polarization beam splitters (PBSs) and two PMs. Light enters the PDPM through the PBS on the left (insertion loss (IL) of 0.2 dB), and is split into orthogonally polarized components that propagate along separate channels. Both channels of the device use polarization-maintaining fiber, and the light in each channel is modulated independently by two different PMs (IL = 2.7 and 3.7 dB). A second fiber PBS (IL = 0.4 dB) recombines light from the two channels to return a phase modulated version of the arbitrarily polarized input signal.

To carry out polarization-independent phase modulation on time-energy entangled photons, the two paths through the PDPM need to be sufficiently indistinguishable so that path

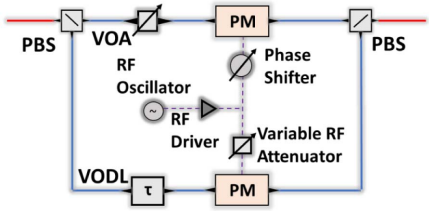

Fig. 1. Schematic of polarization diversity PDPM—single-mode and polarization-maintaining fibers are depicted in red and blue.

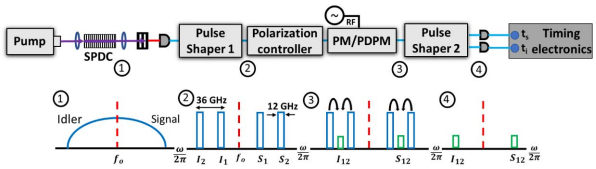

Fig. 2. Experimental setup for measuring frequency-bin entanglement in a BFC. Note that either a standalone PM or PDPM is used to mix frequencies in this arrangement.

information cannot be gleaned from the system [13,14]. Namely, the path length and optical loss through the two arms of the PDPM need to be nearly identical. Furthermore, the RF drive to the two PMs—in terms of modulation depth and RF delay—needs to be matched as well. A variable optical attenuator (VOA, min. IL = 1.5 dB) was tuned until the optical loss through each arm was the same. To determine the path length difference between the arms of the PDPM, broadband light was launched into the PDPM, so that at least some light entered each arm. The output of the PDPM was sampled with a polarizer (oriented at 45° relative to the polarization in PDPM channels) and sent to an optical spectrum analyzer. The path length difference between the arms was estimated from the spacing of the spectral fringes [15]. By suitably adjusting the variable optical delay line (VODL, IL = 1.0 dB), we reduced the path length difference between the arms of the PDPM. We were able to set the relative delay to zero with a precision of ≈60 fs, limited by slow delay fluctuations in the ambient environment. Although there are fluctuations in polarization of photons exiting the PDPM, this does not affect the efficacy of the frequency-bin entanglement measurement as long as polarization-independent single photon detectors are used.

Each PM in the PDPM has its own modulation efficiency (V_π). Consequently, when both modulators are driven with the same RF waveform and continuous wave (CW) optical test signal, frequency combs with slightly different spectra are generated. To ensure that both PMs impart identical phase shifts, an RF attenuator was used to adjust the power delivered to the PM with higher modulation efficiency. To minimize the RF delay between the driving waveforms, the output of the PDPM was sampled in a manner similar to that described above. Any delay between the RF driving waveforms induces a linear spectral phase shift, which manifests as asymmetry in the comb spectrum. An RF phase shifter was used to reduce the RF delay between the driving waveforms.

As currently constructed, the PDPM has an IL of 5.6 dB. However, one of the larger sources of loss stems from the fact that the PMs in the PDPM have different ILs (2.7 and 3.7 dB). Matching their losses to the lower value would shave a decibel off the overall system loss.

After matching both arms of the PDPM, the polarization diversity scheme was used to characterize frequency-bin entanglement in a BFC in a manner similar to that presented in Refs. [6–8], where different frequency modes are mixed using electro-optic phase modulation. If, for example, the frequency of phase modulation equals one-half the free spectral range (FSR) of the BFC, one can project adjacent signal and idler pairs on top of each other, thereby creating an indistinguishable superposition state at frequencies halfway between the original modes (I_{12} and S_{12} in Fig. 2). By varying the joint phase on one of the BFC comb line pairs, it is possible to vary the overall amplitude of this superposition state and, therefore, the probability of detecting coincidences at intermediate frequencies I_{12} and S_{12}. The result is a sinusoidal variation in the number of coincidences as a function of the joint phase on one of the comb line pairs [7].

The setup for carrying out two-photon interferometry and measuring frequency-bin entanglement across comb line pairs is shown in Fig. 2. A CW laser pumps a periodically poled lithium niobate waveguide, which generates a broadband (5 THz) spontaneous parametric downconversion (SPDC) spectrum. A BFC is carved from this continuous spectrum by a pulse shaper ("Pulse Shaper 1," IL = 6 dB). Pulse Shaper 1 was set to yield a BFC with an FSR of 36 GHz, and each frequency mode had a bandwidth of 12 GHz. A polarization controller was placed after the pulse shaper and used to vary the polarization of the BFC at the input of the PDPM (or standalone PM). The PDPM (or standalone PM) was driven at half the FSR of the BFC (18 GHz) in order to overlap adjacent frequency modes. A second pulse shaper ("Pulse Shaper 2," IL = 6 dB) was used to demultiplex the output of the PDPM (or standalone PM) and send signal and idler photons at the intermediate frequencies to a pair of InGaAs single photon detectors. An event timer was used to tag single photon events and generate a histogram of two-photon coincidences.

The losses through the elements in Fig. 2 add up to around 18 dB. However, photonic integration can play a huge role in lowering the component and system losses. For example, a channel in a pulse shaper can be realized with a pair of filters and a phase shifting element between. In a silicon photonics platform, such a device could have an IL less than 0.45 dB [16]. Furthermore, there have been impressive advances in the last year with regard to low loss PMs [10]. Consequently, low loss PDPMs (≈2.0 dB) and pulse shapers (≈0.5 dB) could be realized based on current advances in microfabrication. Photonic integration also makes it possible to achieve phase stability between the arms of the PDPM at no additional cost.

To quantify the benefits of using a polarization diversity scheme, the performance of the PDPM was compared with that of a standalone PM. Both devices were first characterized using linearly polarized light from a CW laser. A deterministic polarization controller (DPC) was used to vary the state of linear polarization at the input port of a standalone PM. The results are illustrated in Fig. 4A. The PM efficiently scatters light into the +1 sideband when the state of polarization is aligned with the slow axis (SA in Fig. 4A) of the PM fiber input. This is the direction that is aligned with the r_{33} electro-optic

coefficient of lithium niobate. As the polarization is tuned toward the fast axis of the PM fiber input (FA in Fig. 4A), some of the light in the PM is now orthogonal to the r_{33} coefficient and passes through the device undergoing substantially reduced phase modulation (factor of 0.14 of original). These experiments were repeated with the PDPM, and the results are shown in Fig. 4D. The polarization diversity scheme functions as expected, and the normalized optical power in the +1 sideband varies from 0.986 to 1 (σ = 0.004).

Two-photon interference measurements were then carried out on a BFC with only two comb-line pairs. In this case, Eq. (1) simplifies to

$$|\Psi\rangle_{\mathrm{BFC}} = \frac{1}{\sqrt{2}}[|1,1\rangle_{SI} + e^{i(\phi_{S2}+\phi_{I2})}|2,2\rangle_{SI}]. \quad \textbf{(2)}$$

For each device—PDPM and standalone PM—interference traces were generated by tracking the coincidence and count rates as a function of the joint phase ($\phi_{S_2} + \phi_{I_2}$) on $|2,2\rangle_{SI}$. For each value of the joint phase, coincidences were recorded over three equal time intervals (5 min intervals for the PDPM and 2 min intervals for the standalone PM). The average number of coincidences and their standard deviation over these three intervals were calculated after subtracting accidentals. Due to the high system losses enumerated above, as well as the low efficiency of our detectors (10% and 20%), the rate of accidentals was three to four times that of coincidences. The full interference traces, for nine different values of the joint phase, are shown in Fig. 3. For the standalone PM, two-photon interference traces were generated for three different polarization states of the BFC—0°, 90°, and an orientation roughly between these states. These angles are defined relative to the slow axis of the PM fiber input, which is polarization-maintaining. As the polarization of the BFC is tuned away from 0°, the number of counts at the overlap frequencies (I_{12} and S_{12}) is expected to fall, as the component of the wavefunction aligned with the r_{33} EO coefficient gets smaller and smaller. As expected, the number of coincidences falls off at a sharp rate, resulting in lower fringe amplitude. When the BFC is aligned with the FA of the PM fiber input (dotted lines in Fig. 3A), the count rate (red) is reduced to 0.28 of that when the BFC is aligned with the SA (solid lines in Fig. 3A). The recorded coincidences (blue) from the BFC are reduced to a factor of 0.07, compared to when the BFC is aligned with the SA. For the PDPM, an interference trace was recorded for the case where photons are equally likely to end up in either arm of the device (dashed lines in Fig. 3B). To see if there was any residual polarization dependence, an interference trace was then recorded for a case where all the photons passed through only one arm of the device (solid lines in Fig. 3B). A drift in the setup over the long acquisition time (around 3 h) may be responsible for some of the differences between the traces in Fig. 3B. However, the polarization diversity scheme is clearly more robust to changes in BFC polarization. The count and coincidence rates for the PDPM are lower compared to that of the standalone PM (BFC polarization at 0°), because the polarization diversity scheme has a higher IL.

Having established that the PDPM can be used to visualize strong two-photon interference in a BFC, regardless of polarization, we now quantify its performance and contrast it with that of a standalone PM. For these measurements, we varied the BFC polarization state using a DPC while keeping the joint

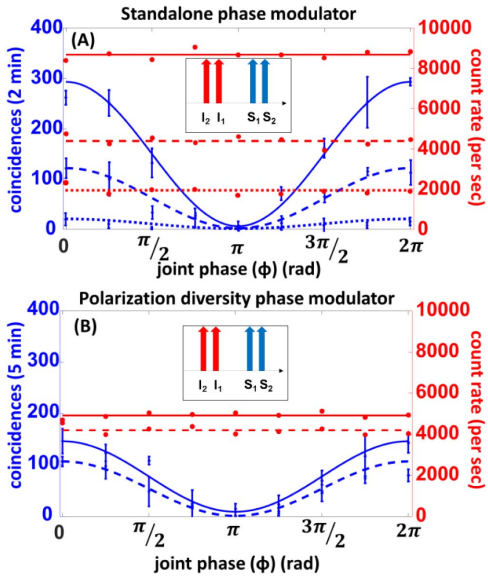

Fig. 3. Results from frequency-bin entanglement measurements. (A) Coincidences (blue) and counts (red) when using the standalone PM for three different orientations of the polarization—0° (solid), 90° (dotted), and an intermediate state (dashed). (B) Coincidences and counts when using the PDPM for two cases—one where photons are equally likely to be in either arm (dashed) and the other where photons go entirely through one arm (solid). The insets show the relative orientation between the polarization of signal and idler bins.

phase on $|2,2\rangle_{SI}$ set to 0, which is the value for which coincidences at the overlap frequencies are expected to be at a maximum. The results are presented in Figs. 4B and 4C, and show that the count and coincidence rates are sensitive to BFC polarization. For measurements with the PDPM, the count and coincidence rates are relatively immune to changes in BFC polarization (Figs. 4E and 4F). The results from classical measurements (Figs. 4A and 4D) were used to determine the expected change in the count and coincidence rates as a function of BFC polarization. The counts are expected to track with the power scattered into the +1 sideband in classical experiments. Coincidences, on the other hand, are expected to fall off quadratically with respect to the drop in power in the +1 sideband. Based on these relationships, the expected change in the normalized count and coincidence rates is plotted (black lines) alongside the actual change in count and coincidence rates. There is good agreement between the data from classical measurements and that from two-photon interferometry. Finally, the measurements using the PDPM were repeated, but with the joint phase on $|2,2\rangle_{SI}$ set to π (hollow markers in Figs. 4E and 4F). Coincidences at the intermediate frequencies are expected to be at a minimum for this value of the joint phase (see Fig. 3), which is what was observed. These measurements were made to establish that the coincidences in Fig. 4E are the result of two-photon interference and not the result of leakage from the original signal and idler bins.

Thus far, two-photon interference measurements were performed on co-polarized signal-idler pairs. However, it is important that any polarization diversity scheme be sufficiently robust to also handle instances where the entangled photons are orthogonally polarized with respect to one another. Since a standalone PM can only modulate one polarization component

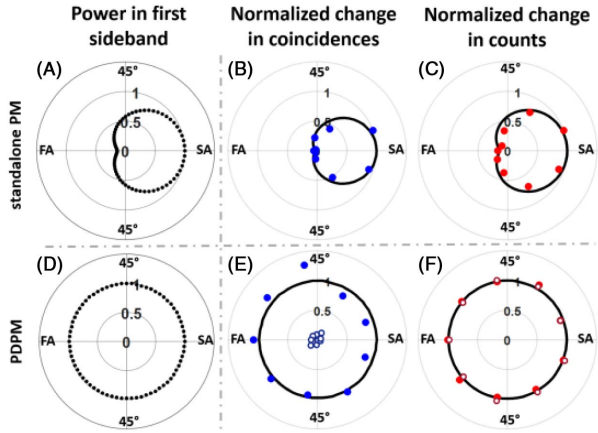

Fig. 4. (A), (D) show the change in power scattered into the +1 sideband as a function of polarization for a standalone PM and the PDPM. (B), (C) show the change in coincidence and count rates for frequency-bin entanglement measurements using a standalone PM. (E), (F) are analogous to (B), (C), but for the PDPM, and include data for two values of the joint phase—$\phi_{S_2} + \phi_{I_2} = 0$ (solid) and $\phi_{S_2} + \phi_{I_2} = \pi$ (hollow). The results are plotted on an azimuthal slice of the Poincaré sphere corresponding to linearly polarized light. (SA, slow axis; FA, fast axis).

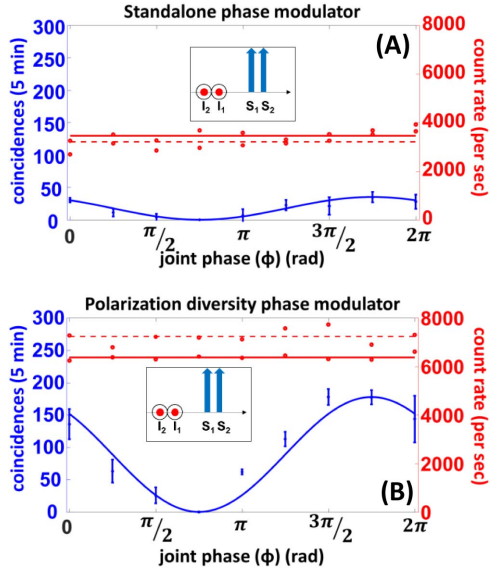

Fig. 5. Frequency-bin entanglement measurements on orthogonally polarized signal-idler pairs using (A) a standalone PM and (B) the PDPM. The dashed and solid red lines correspond to the signal and idler count rates, respectively. The insets show the relative orientation between the polarization of the signal and idler bins.

at a time, we expect that its ability to efficiently mix frequencies of orthogonally polarized signal-idler pairs will be limited.

To prepare orthogonally polarized signal-idler pairs, we took advantage of frequency dependent polarization rotation in a birefringent fiber. Our SPDC spectrum was carved into a BFC consisting of signals and idlers 1.3 THz apart from each other, with the $S_1 - S_2$ and $I_1 - I_2$ spacing kept at 36 GHz. The resulting BFC was launched at 45° relative to the slow axis of a 28 cm section of polarization-maintaining fiber (with an estimated differential group delay of 1.73 ps/m). The signal-idler spacing was chosen so that the number of Poincaré sphere rotations undergone by the signal and idler polarizations differed by one-half rotation at the output of the section of polarization-maintaining fiber. Interference traces similar to those recorded in Fig. 3 were then generated, but with the signal and idler polarizations orthogonal to one another. Figure 5 shows that the amplitude of the two-photon trace generated using a standalone PM is very low since a standalone PM is unable to efficiently mix the frequencies of both signal and the idler photons simultaneously. The PDPM is clearly not limited in this regard.

In this Letter, we have clearly shown that the PDPM can be used to measure frequency-bin entanglement in the presence of polarization scrambling, as occurs over fiber-optic channels. In addition, we established that frequency-bin entanglement can also be measured in cross-polarized signal-idler pairs—a requirement for working with states also entangled in polarization. These results, coupled with current advances in photonic integration, show the PDPM to be a promising tool for future quantum networks based on fiber-optic infrastructure.

Funding. Army Research Laboratory (ARL) (W911NF-17-2-0003).

†These authors contributed equally to this Letter.

REFERENCES

1. J. T. Barreiro, T.-C. Wei, and P. G. Kwiat, Nat. Phys. **4**, 282 (2008).
2. T. M. Graham, H. J. Bernstein, T.-C. Wei, M. Junge, and P. G. Kwiat, Nat. Commun. **6**, 7185 (2015).
3. S. P. Walborn, S. Pádua, and C. H. Monken, Phys. Rev. A **68**, 042313 (2003).
4. C. Schuck, G. Huber, C. Kurtsiefer, and H. Weinfurter, Phys. Rev. Lett. **96**, 190501 (2006).
5. J. M. Lukens and P. Lougovski, Optica **4**, 8 (2017).
6. M. Kues, C. Reimer, P. Roztocki, L. R. Cortés, S. Sciara, B. Wetzel, Y. Zhang, A. Cino, S. T. Chu, B. E. Little, D. J. Moss, L. Caspani, J. Azaña, and R. Morandotti, Nature **546**, 622 (2017).
7. P. Imany, J. A. Jaramillo-Villegas, O. D. Odele, K. Han, D. E. Leaird, J. M. Lukens, P. Lougovski, M. Qi, and A. M. Weiner, Opt. Express **26**, 1825 (2018).
8. P. Imany, O. D. Odele, J. A. Jaramillo-Villegas, D. E. Leaird, and A. M. Weiner, Phys. Rev. A **97**, 1 (2018).
9. E. L. Wooten, K. M. Kissa, A. Yi-Yan, E. J. Murphy, D. A. Lafaw, P. F. Hallemeier, D. Maack, D. V. Attanasio, D. J. Fritz, G. J. McBrien, and D. E. Bossi, IEEE J. Sel. Top. Quantum Electron. **6**, 69 (2000).
10. C. Wang, M. Zhang, X. Chen, M. Bertrand, A. Shams-Ansari, S. Chandrasekhar, P. Winzer, and M. Lončar, Nature **562**, 101 (2018).
11. H. Fukuda, K. Yamada, T. Tsuchizawa, T. Watanabe, H. Shinojima, and S.-I. Itabashi, Opt. Express **16**, 4872 (2008).
12. C. Haffner, D. Chelladurai, Y. Fedoryshyn, A. Josten, B. Baeuerle, W. Heni, T. Watanabe, T. Cui, B. Cheng, S. Saha, D. L. Elder, L. R. Dalton, A. Boltasseva, V. M. Shalaev, N. Kinsey, and J. Leuthold, Nature **556**, 483 (2018).
13. M. Brodsky, E. C. George, C. Antonelli, and M. Shtaif, Opt. Lett. **36**, 43 (2011).
14. D. E. Jones, B. T. Kirby, and M. Brodsky, npj Quantum Inf. **4**, 58 (2018).
15. A. Weiner, *Ultrafast Optics* (Wiley, 2011), vol. **72**.
16. AIM Photonics, "Silicon photonics process design kit (APSUNY PDKv2.5a)," http://www.aimphotonics.com/pdk/.